Geosynthetic reinforced soil bridge abutments under base motion dynamic loading

Mehdi Askari[1*], Jaber Mamaghanian[2], Hamid Reza Razeghi[3], S. Mustapha Rahmaninezhad[4]

[1] Formerly Post-graduate student, School of Civil Engineering, Iran University of Science and Technology, Tehran, Iran

[2] Postdoctoral Researcher and Research Associate, School of Civil Engineering, Iran University of Science and Technology, Tehran, Iran

[3] Associate Professor, School of Civil Engineering, Iran University of Science and Technology, Tehran, Iran.

[4] Geotechnical Department, Terracon Consulting Inc., 1506 Mid Cities Dr, Pharr, TX 78577, USA

*Corresponding author: Mehdiaskari.eng951@gmail.com

doi: https://doi.org/10.21467/proceedings.112.15

ABSTRACT

Geosynthetic reinforced soil (GRS) bridge abutments are of great interest in different highway projects due to their ease of construction, flexibility, cost-saving, aesthetic aspects and good performance comparing to traditional ones. However, their seismic performance is of question due to their complex structure and lack of proper investigations. Therefore, this paper investigates GRS abutment performance under earthquake loading through numerical modelling using FLAC software. The effect of lateral restraint due to the bridge deck existence was analyzed in this study. Comparing the models with and without the bridge deck indicated that the bridge deck simulation affected static and seismic performance of GRS abutment considerably. Accordingly, restriction of the upper part of GRS abutment with bridge deck modelling decreased facing displacement and reinforcement loads considerably under static loading. Furthermore, simulation of bridge deck caused a noticeable reduction in facing displacement after seismic loading, while it had no considerable effects in reinforcement loads. Additionally, it was found that seismic loading imposed a great increase in facing displacement and reinforcement loads compared to static state. Therefore, it is crucial to investigate the dynamic performance of GRS abutments constructed in seismic prone areas.

Keywords: Geosynthetics, GRS bridge abutment, Dynamic analysis, Geogrid, Numerical analysis, FLAC

1 Introduction

Geosynthetic reinforced soil (GRS) bridge abutments could be considered as a particular type of GRS walls that support the bridge deck and carry live loads through two shallow strip foundations (sill) on the top of two symmetric GRS walls. The main difference between regular GRS walls and GRS abutment is that the latter usually bear a higher surcharge loading level subjected to the near the top of the wall facing (Wu et al. 2006). Through recent years, the GRS abutments with the flexible segmental wall facing have been successfully implemented as a permanent structure in the transportation sector due to the many edges over their rivals. GRS abutments are easier to construct, economical in both construction and maintenance, and more flexible than other types of abutments. Besides, the studies on the GRS abutments static behavior have shown satisfactory performance in terms of horizontal deformation and reinforcement loads (Fakharian and Attar 2007; Zheng and Fox 2017; Zheng et al. 2018a; Zheng et al. 2018b). However, the seismic performance of such structures has remained to be investigated.

Several experimental investigations have been conducted on the dynamic behavior of GRS walls and abutments through these years. Helwany et al. (2012) and (Zheng et al. 2019) experimentally investigated the dynamic

Proceedings DOI: 10.21467/proceedings.112; Series: AIJR Proceedings; ISSN: 2582-3922; ISBN: 978-81-947843-3-3

response of reduced-scaled GRS walls and abutments using shaking table tests. However, fewer studies focused specifically on the dynamic response of GRS abutments with a numerical approach. Nevertheless, numerical investigations on GRS walls dynamic behavior can be used as background studies to enlighten GRS abutments dynamic performance. The studies done by Zarnani et al. (2011) and El-Emam et al. (2001) on a GRS wall revealed a pattern of the facing lateral displacements and geogrid strains under seismic excitation. Ling et al. (2004) and later Ling et al. (2005) also numerically analyzed the effects of reinforcement vertical spacing and excitation properties on the residual facing lateral displacements. Some studies also focused on the effects of seismic motions inherent characteristics on the response of GRS walls (Ling et al. 2010; Murali Krishna and Bhattacharjee 2016). Few studies also have specifically concentrated on the dynamic numerical analysis of GRS abutments. Fakharian and Attar (2007) reported that the GRS abutment with the same characteristics carefully monitored and reported by Abu-Hejleh et al. (2001) significantly underwent an increase in facing displacements after base acceleration was applied. Moreover, Ghaderi et al. (2017) carried out an extensive parametric study through dynamic Finite Element (FE) Analysis on the GRS abutment to obtain an analytical equation for an optimal design procedure of such structures in dynamic condition. There are also several studies using an analytical procedure to evaluate the limit state condition in static analysis and optimize the conventional design methods. These studies were mostly conducted on the GRS walls. A surcharge load on the top of GRS wall was considered in some of them (Blatz and Bathurst 2003; Xie and Leshchinsky 2015; Xie et al. 2016). Ausilio (2014) analyzed the bearing capacity of strip footing in the GRS wall crest vicinity utilizing the kinematic theorem of limit analysis in the earthquake condition. As can be inferred, fewer investigations were performed on the dynamic analysis of the GRS abutments.

In the current study, a verified numerical procedure by using the two-dimensional plane strain Finite Difference (FD) Fast Lagrangian Analysis of Continua (Flac) V.7.0 program (Itasca 2001) was adopted to simulate and analyze a GRS abutment after construction and under a harmonic base acceleration. The numerical model of GRS abutment representing the real field condition, consisting of two GRS walls and the bridge deck, which spans between two walls, was developed to assess the effects of lateral constraint due to the existence of bridge deck on the top of GRS abutments.

2 Numerical model verification

The shaking table test results on the RMC 1/6-scaled GRS wall with 1 m height (Figure 1), instrumented and monitored by El-Emam and Bathurst (2004), was assigned to verify the numerical analysis procedure. To investigate the effects of toe contribution to lateral load-bearing, the wall was constructed and analyzed with two toe conditions. It was first modeled with hinged toe condition, and then it was modeled with free toe condition. Tables 1 and 2 describe the materials and interface properties used in RMC wall, respectively. The backfill soil was modeled with Cap-Yield (CY) soil constitutive model based on the hardening plasticity theorem. By adopting such a constitutive model for backfill soil, the nonlinear behavior of soil during loading/unloading and then reloading during dynamic base acceleration can be implemented precisely. The geogrid PET and facing panel also were modeled by the linear elastic-plastic model. Interface between backfill-facing also was assigned to be linear springer-slider with the Mohr-Coulomb failure criterion model of FLAC program. It is noteworthy to mention that the contact between geogrid and backfill soil was considered rigid to prevent the potential slippage between geogrids and backfill soil zones. After modelling step-by-step construction sequences, a stepped-amplitude sinusoidal input base acceleration with a 5 Hz frequency velocity

Proceedings DOI: 10.21467/proceedings.112
ISBN: 978-81-947843-3-3

Series: AIJR Proceedings
ISSN: 2582-3922

was applied at the bottom boundary. The inputted acceleration amplitude increases 0.05g every 5 seconds. The full description of the RMC wall can be found in the study conducted by El-Emam and Bathurst (2004).

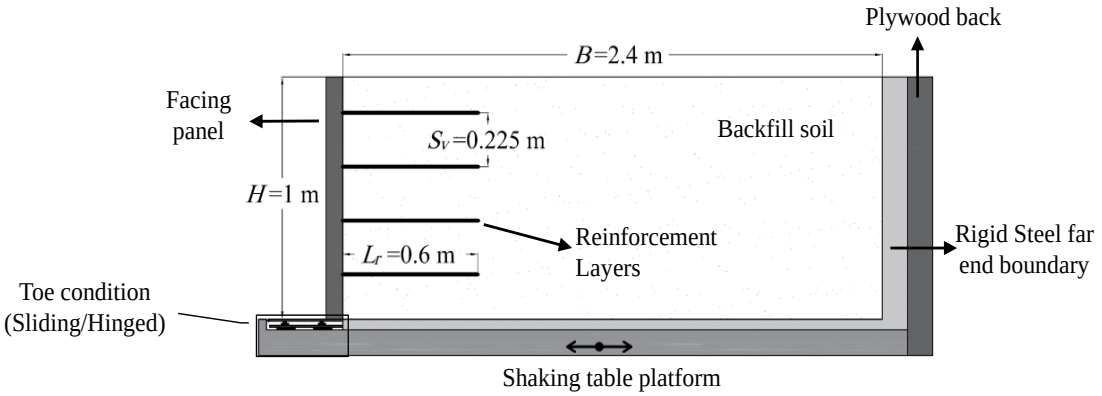

Figure 1. Schematic cross section of constructed RMC wall.

Table 1. Backfill soil and geogrids properties for RMC wall

Backfill soil	
Properties	Values
Unite weight (γ : kN/m^3)	15.7
Reference tangent shear modulus (G^e_{ref} : MPa)	211.5
Reference bulk modulus (K^{iso}_{ref} : MPa)	57.5
Poisson ratio (υ)	0.3
Constant failure ratio (R_f)	0.93
Plastic strain coefficient (m)	1
Friction angle (φ'_f : degree)	54
Cohesion (C: kPa)	0
Dilation angle (ψ : degree)	14.5
Reinforcement	
Properties	Values
Thickness (mm)	2
Stiffness (J: kN/m)	90
Ultimate strength (kN/m)	13

Table 2. Interface properties for numerical simulation of RMC wall

Interface	Friction angle (δ_{bond})	Cohesion (C_{bond} : kPa)	Normal stiffness (K_{nbond} : MN/m)	Shear stiffness (K_{sbond} : MN/m)
Soil-Facing	40.5	0	100	60

As shown in Figures 2 and 3, the predicted values for geogrid connection loads at the end of construction and ascending levels of base acceleration amplitude and wall facing displacement time history were in good

agreement with measured results. However, some discrepancies can be detected between numerical and measured values of connection loads in the upper geogrids in some cases, which might be due to the linear elastic model of reinforcement and rigid interfaces defined between geogrids and backfill soil.

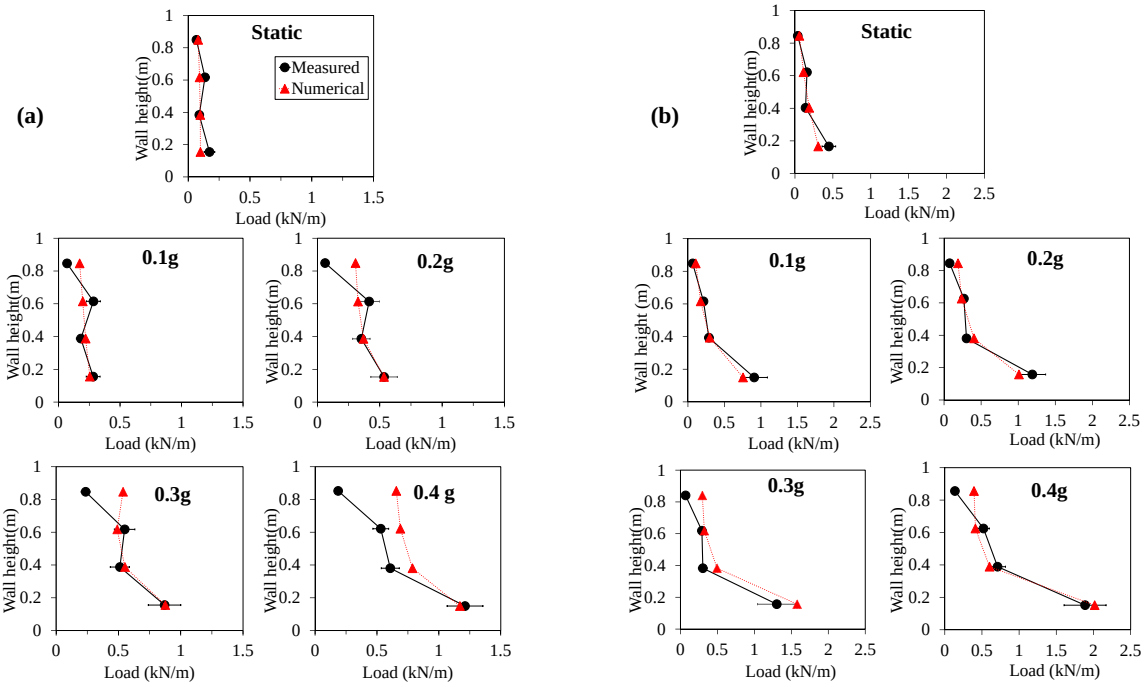

Figure 2. Measured and predicted geogrids connection loads of RMC Wall at static condition and under seismic loading: (a) hinged toe condition, and (b) free toe condition.

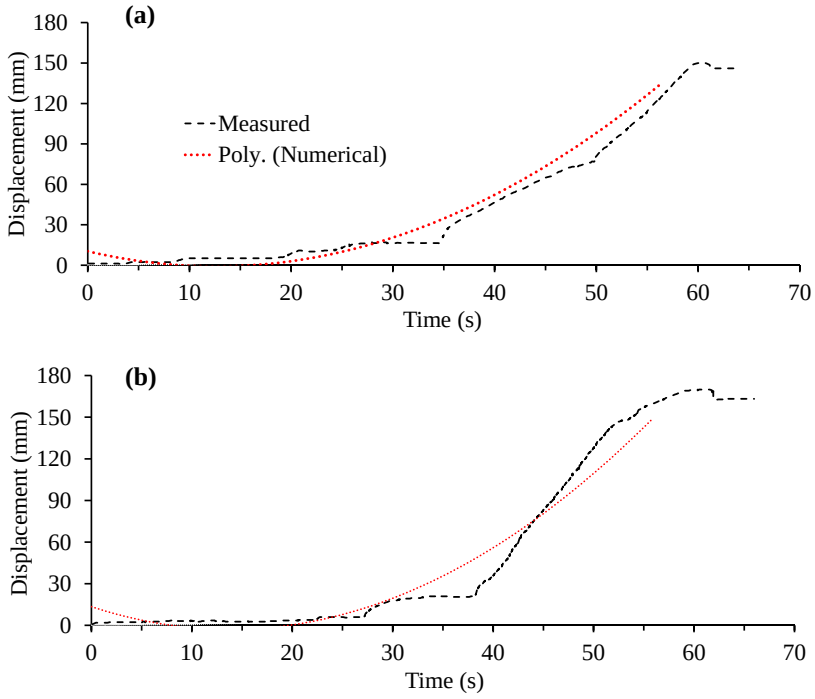

Figure 3. Measured and predicted time histories of lateral displacements at top of RMC Wall under seismic loading: (a) hinged toe condition, and (b) free toe condition.

Proceedings DOI: 10.21467/proceedings.112
ISBN: 978-81-947843-3-3

Series: AIJR Proceedings
ISSN: 2582-3922

3 Numerical modelling of GRS abutment

3.1 Materials

The verified numerical procedure was then utilized to simulate and analyze the GRS bridge abutment at both ends of construction and dynamic stages. The GRS bridge abutment system in the current study was first examined in Zheng and Fox (2016) study. The system contains two GRS bridge abutment and a single span concrete deck sitting on the sills supported by GRS abutments (Figure 4). As it was practiced in the verification section, the SW/SP backfill soil based on the Unified Soil Classification System with 95.0% relative compaction was modeled with continuum zones and the CY soil model. The calculated backfill soil properties were derived based on the properties presented in Zheng and Fox (2016). The dense sand of foundation soil below the GRS abutments was also modeled with the linear elastic-perfectly plastic model with the Mohr-Coulomb failure criterion. Additionally, segmental modular blocks for facing, sill and deck were also considered linear elastic. The geogrid PET was modeled with the linear elastic-plastic constitutive model and two-dimensional structural cable elements in FLAC. Moreover, 5.0% of material damping was allocated to the whole model for the dynamic analysis phase. Table 3 summarizes the properties of materials used in the numerical modelling of GRS abutment.

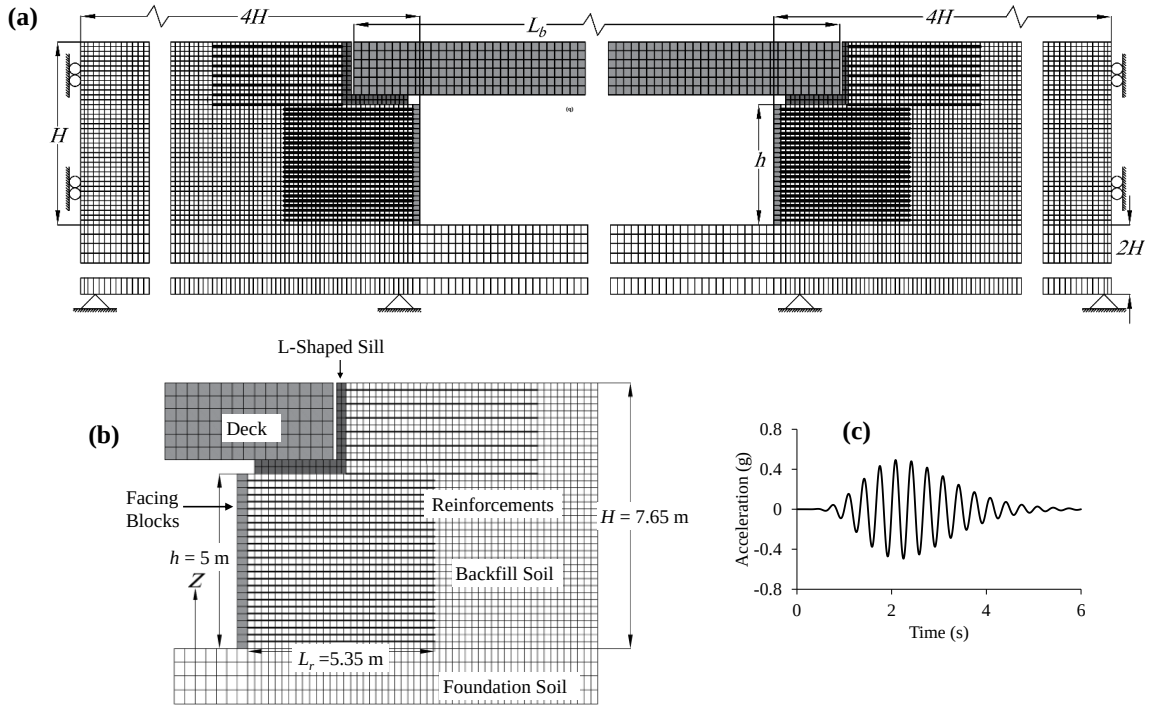

Figure 4. Finite-Difference discretization and boundary conditions of GRS abutments system: (a) whole GRS bridge abutment system, (b) details of GRS walls, and (c) base excitation acceleration time history.

The linear spring-slider model with the Mohr-Coulomb failure criterion was considered to model interfaces between different materials (Table 4). Also, the geogrid nodes were rigidly attached to the backfill soil grids.

3.2 Construction sequences and loading procedure

The sequential stages of construction were exactly reproduced to provide a real-field condition for the whole simulation. As mentioned earlier, this study intention was to evaluate the effects of simulation of the bridge

deck on the static and dynamic performance of the GRS abutment. To this aim, two GRS abutment and spanning deck firstly modeled and analyzed (HR model). Then, a GRS abutment modeled without the bridge deck, and only the surcharge load equivalent with the deck weight was applied on the top of the GRS abutment (NHR model). The modelling procedure for both cases was kept the same. After the foundation soil placement (Stage 1), the lower GRS wall with the height of h = 5 m was constructed within 25 backfilling lifts (Stage 2). Each layer consisted of 200 mm backfill soil, geogrid layer and facing block. Thereafter, the sill and the bridge deck in the HR model were placed (Stage 3), and then the upper GRS wall was modeled within 12 lifts (Stage 4). Finally, the pavement layer of the approach road was simulated (Stage 5). It is noteworthy to mention that in each stage and within stages 2 and 4, each layer of backfilling the whole model was solved to reach a numerical equilibrium.

Table 3. Material properties for numerical simulation of GRS abutment.

Backfill soil	
Properties	Values
Unite weight (γ : kN/m^3)	22.1
Reference tangent shear modulus (G^e_{ref} : MPa)	9.61
Reference bulk modulus (K^{iso}_{ref} : MPa)	7.5
Poisson ratio (υ)	0.3
Constant failure ratio (R_f)	0.93
Plastic strain coefficient (m)	1
Friction angle (φ'_f : degree)	36
Cohesion (C: kPa)	0
Dilation angle (ψ : degree)	3.8
Reinforcement	
Properties	Values
Thickness (mm)	2
Stiffness (J: kN/m)	1000
Ultimate strength (kN/m)	180
Facing modular blocks, sill and bridge deck	
Properties	Values
Elastic modulus (GPa)	20
Poisson ratio	0.2

Table 4. Interface properties for numerical simulation of GRS bridge abutment

Interfaces	Friction angle (δ_{bond})	Cohesion (C_{bond} : kPa)	Normal stiffness (K_{nbond} : MN/m)	Shear stiffness (K_{sbond} : MN/m)
Block-Block	57	46	1000	40
Soil-Block	25.2	0	100	1
Toe	85	0	3000	200
Sill-Soil	60	0	1000	10
Sill-Deck	40	0	100	5

Proceedings DOI: 10.21467/proceedings.112
ISBN: 978-81-947843-3-3

Series: AIJR Proceedings
ISSN: 2582-3922

At the end of construction, a sinusoidal base acceleration with variable amplitude with the following correlation was applied to the bottom boundary of the numerical model in terms of the horizontal velocity function (Figure 4c).

$$u_t = \frac{k}{2} \times \sqrt{\beta . e^{-\alpha t} t^{\xi}} \times \sin(2\pi f t) \quad (2)$$

where the peak acceleration amplitude is $k = 0.5g$, constant coefficients of the input function are $\xi = 12$, $\beta = 55$ and $\alpha = 5.5$, input motion frequency f=3 Hz and the duration of base motion is t = 6 s.

3.3 Model mesh and boundary conditions

Figures 4a and 4b provides the details of the FD mesh of the GRS abutment numerical model. The numerical meshes were somehow employed to the whole model to reach an optimal balance between numerical model accuracy and time of numerical solution. Moreover, the criterion introduced by Kuhlemeyer and Lysmer (1973) of the maximum mesh dimension was also taken into consideration. The maximum dimension of the biggest grid zone of the current model did not exceed $\lambda/10$, where λ = 36 m is the wavelength of base motion. Furthermore, the boundary conditions of the model in the static analysis are depicted in Figure 4a. After construction and at the beginning of the dynamic analysis, the boundary conditions at the bottom boundary changed from fixed in both vertical and horizontal directions to only fixed in the vertical direction to provide horizontal compliance when the base motion was applied. Additionally, the lateral boundaries at two far-ends were changed from horizontally fixed to the free-field boundary to avoid the wave reflection into the model. Of note, to diminish the boundary effects on the numerical results, the lateral and bottom boundaries were located within a proper distance from the facing (4*H*) and base level of the lower GRS wall (2*H*), respectively.

4 Numerical modelling results

The GRS bridge abutment system was numerically evaluated with the lateral constraint due to simulation of bridge deck (HR model) and without it (NHR model) in terms of the facing lateral displacements, the maximum reinforcement loads, reinforcement connection loads, and sill horizontal deflection, settlement and rotation at the end of construction (EOC) and after the dynamic load was applied (PD).

The facing lateral displacements, maximum reinforcement loads and reinforcement connection loads are shown in Figure 5 at EOC, and PD, deducted from those at EOC. It indicates that the dynamic load significantly increased the facing lateral displacements and geogrid load level compared to those at EOC in both HR and NHR models. The results of the HR model presents that facing lateral displacements were markedly decreased due to the lateral constraint of the top of the wall at both EOC and PD by about 21.0% and 58.0%, respectively. However, modelling the bridge deck in HR model caused a noticeable decrease in both maximum loads and connection loads uniformly at EOC. This level of reinforcement load reduction was not observed at PD state, though. Moreover, by comparing the results of GRS abutment at EOC and PD states (in both HR and NHR models), it can be found that the seismic loading could impose a considerable increase in facing displacements and reinforcement loads and it may lead to the serviceability problems of the structure. On average, the facing displacements, maximum geogrid loads and geogrid connection loads increased by 80%, 45% and 50% respectively after seismic loading in HR model. Therefore, it is vital to investigate the dynamic performance of GRS abutments in seismic prone areas.

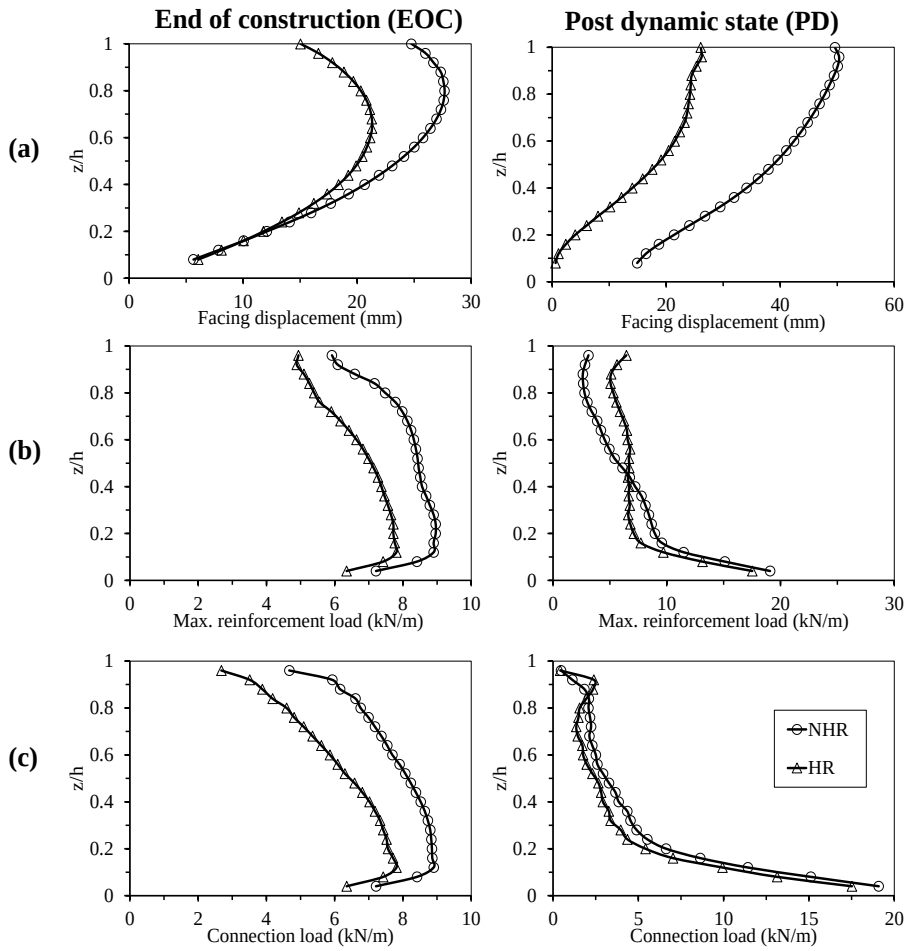

Figure 5. Predicted results of numerical simulation for HR and NHR modelling at EOC and PD states: (a) facing lateral displacement, (b) maximum reinforcement loads, and (c) geogrid-facing connection loads.

Table 5. The effects of lateral restraint of the lower GRS walls on the sill deflection, settlement and rotation at EOC and PD states.

Analysis condition	Sill horizontal deflection	Sill settlement	Sill Rotation
HR/EOC	0.5 mm	29.3 mm	0. 03%
NHR/EOC	25.8 mm	36.5 mm	0. 53%
HR/PD	56.8 mm	40.1 mm	0.02%
NHR/PD	90.1 mm	43.2 mm	0.4%
Reduction/EOC	98.0%	19.0%	94.0%
Reduction/PD	37.0%	7.0%	93.0%

As a reference, Table 5 details the values of horizontal sill deflection, settlement and rotation in the HR and NHR models and their reduction at both EOC and PD states. The sill deflection and rotation obey the fact that the lateral constraint due to the bridge deck in HR model caused less lateral movement of the top of wall

Proceedings DOI: 10.21467/proceedings.112
ISBN: 978-81-947843-3-3

Series: AIJR Proceedings
ISSN: 2582-3922

at EOC and PD states. However, the sill settlement was not affected by modelling of the bridge deck in HR model in comparison with the results in NHR model.

5 Conclusion

Based on the results of this study it can be concluded that modelling of bridge deck has considerable effects on the performance evaluation of GRS abutments in both static state and after dynamic (i.e. seismic) loading. It was found that neglecting effects of bridge deck led to overestimation of facing displacements, maximum reinforcement loads and geogrid-facing connection loads. Hence it is vital to consider effects of bridge deck to evaluate the performance of GRS abutments in an effective manner. Further, as the seismic loading imposed a considerable increase in facing displacement and reinforcement loads, its effect should be considered in GRS abutments constructed at seismic prone areas.

How to Cite this Article:

Askari, M., Mamaghanian, J., Razeghi, H. R., & Rahmaninezhad, S. M. (2021). Geosynthetic reinforced soil bridge abutments under base motion dynamic loading. *AIJR Proceedings*, 119-128.

References

Abu-Hejleh N, Zornberg JG, Wang T, and McMullen M. 2001. Performance of geosynthetic-reinforced walls supporting the Founders/Meadows Bridge and approaching roadway structures. Report 2: Assessment of the performance and design of the front GRS walls and recommendations for future GRS abutments.

Ausilio E. 2014. Seismic Bearing Capacity of Strip Footings Located Close to the Crest of Geosynthetic Reinforced Soil Structures. Geotechnical and Geological Engineering 32(4):885-899.

Blatz JA, and Bathurst RJ. 2003. Limit equilibrium analysis of large-scale reinforced and unreinforced embankments loaded by a strip footing. Canadian Geotechnical Journal 40(6):1084-1092.

El-Emam M, Bathurst R, Hatami K, and Mashhour M. 2001. Shaking table and numerical modelling of reinforced soil walls. Proceedings of the International Symposium on Earth Reinforcement, IS Kyushu. p 329-334.

El-Emam MM, and Bathurst RJ. 2004. Experimental design, instrumentation and interpretation of reinforced soil wall response using a shaking table. International Journal of Physical Modelling in Geotechnics 4(4):13-32.

Fakharian K, and Attar I. 2007. Static and seismic numerical modelling of geosynthetic-reinforced soil segmental bridge abutments. Geosynthetics International 14(4):228-243.

Ghaderi R, Helwany S, Wu JT, Meinholz P, and Alizadeh V. 2017. Seismic Behavior of Geosynthetic-Reinforced Soil (GRS) Bridge Abutments with Concrete Block Facing—an Analytical Study. Transportation Infrastructure Geotechnology 4(2-3):52-83.

Helwany S, Wu J, and Meinholz P. 2012. Seismic design of geosynthetic-reinforced soil bridge abutments with modular block facing.

Itasca. 2001. FLAC—Fast Lagrangian Analysis of Continua. Version 4.00. ed.

Kuhlemeyer RL, and Lysmer J. 1973. Finite element method accuracy for wave propagation problems. Journal of Soil Mechanics & Foundations Div 99(Tech Rpt).

Ling HI, Liu H, Kaliakin VN, and Leshchinsky D. 2004. Analyzing dynamic behavior of geosynthetic-reinforced soil retaining walls. Journal of Engineering Mechanics 130(8):911-920.

Ling HI, Liu H, and Mohri Y. 2005. Parametric studies on the behavior of reinforced soil retaining walls under earthquake loading. Journal of engineering mechanics 131(10):1056-1065.

Ling HI, Yang S, Leshchinsky D, Liu H, and Burke C. 2010. Finite-element simulations of full-scale modular-block reinforced soil retaining walls under earthquake loading. Journal of engineering mechanics 136(5):653-661.

Murali Krishna A, and Bhattacharjee A. 2016. Behavior of Rigid-Faced Reinforced Soil-Retaining Walls Subjected to Different Earthquake Ground Motions. International Journal of Geomechanics 17(1):06016007.

Wu JT, Lee KZ, and Pham T. 2006. Allowable bearing pressures of bridge sills on GRS abutments with flexible facing. Journal of Geotechnical and Geoenvironmental Engineering 132(7):830-841.

Xie Y, and Leshchinsky B. 2015. MSE walls as bridge abutments: Optimal reinforcement density. Geotextiles and Geomembranes 43(2):128-138.

Xie Y, Leshchinsky B, and Yang S. 2016. Evaluating reinforcement loading within surcharged segmental block reinforced soil walls using a limit state framework. Geotextiles and Geomembranes 44(6):832-844.

Zarnani S, El-Emam MM, and Bathurst RJ. 2011. Comparison of numerical and analytical solutions for reinforced soil wall shaking table tests. Geomechanics and Engineering 3(4):291-321.

Zheng Y, and Fox PJ. 2016. Numerical Investigation of Geosynthetic-Reinforced Soil Bridge Abutments under Static Loading. Journal of Geotechnical and Geoenvironmental Engineering 142(5):04016004.

Zheng Y, and Fox PJ. 2017. Numerical Investigation of the Geosynthetic Reinforced Soil–Integrated Bridge System under Static Loading. Journal of Geotechnical and Geoenvironmental Engineering 143(6):04017008.

Zheng Y, Fox PJ, and McCartney JS. 2018a. Numerical Simulation of Deformation and Failure Behavior of Geosynthetic Reinforced Soil Bridge Abutments. Journal of Geotechnical and Geoenvironmental Engineering 144(7):04018037.

Zheng Y, Fox PJ, and McCartney JS. 2018b. Numerical study on maximum reinforcement tensile forces in geosynthetic reinforced soil bridge abutments. Geotextiles and Geomembranes 46(5):634-645.

Zheng Y, McCartney JS, Shing PB, and Fox PJ. 2019. Physical model tests of half-scale geosynthetic reinforced soil bridge abutments. II: Dynamic loading. Journal of Geotechnical and Geoenvironmental Engineering 145(11):04019095.

Proceedings DOI: 10.21467/proceedings.112
ISBN: 978-81-947843-3-3

Series: AIJR Proceedings
ISSN: 2582-3922